

Status of the plasma generator of the superconducting proton linac

M. Kronberger, D. Faircloth, J. Lettry, M. Paoluzzi, H. Pereira et al.

Citation: *Rev. Sci. Instrum.* **83**, 02A703 (2012); doi: 10.1063/1.3662478

View online: <http://dx.doi.org/10.1063/1.3662478>

View Table of Contents: <http://rsi.aip.org/resource/1/RSINAK/v83/i2>

Published by the [American Institute of Physics](#).

Related Articles

Experimental investigation on focusing characteristics of a He-Ne laser using circular Fresnel zone plate for high-precision alignment of linear accelerators

Rev. Sci. Instrum. **83**, 053301 (2012)

Frequency control in the process of a multicell superconducting cavity production

Rev. Sci. Instrum. **83**, 043304 (2012)

Upgrade of the MIT Linear Electrostatic Ion Accelerator (LEIA) for nuclear diagnostics development for Omega, Z and the NIF

Rev. Sci. Instrum. **83**, 043502 (2012)

Phase sensitive monitoring of electron bunch form and arrival time in superconducting linear accelerators

Appl. Phys. Lett. **100**, 141103 (2012)

Experimental demonstration of wakefield effects in a THz planar diamond accelerating structure

Appl. Phys. Lett. **100**, 132910 (2012)

Additional information on Rev. Sci. Instrum.

Journal Homepage: <http://rsi.aip.org>

Journal Information: http://rsi.aip.org/about/about_the_journal

Top downloads: http://rsi.aip.org/features/most_downloaded

Information for Authors: <http://rsi.aip.org/authors>

ADVERTISEMENT

**EMBEDDED
PLANET**



Custom MicroTCA system integration.
Embedded Planet and Schroff.
Embedded Planet CPU with any DSP,
FPGA, storage or power.
Custom RTM or AMC designs.

www.embeddedplanet.com
866.612.7865

Schroff[®]



Status of the plasma generator of the superconducting proton linac^{a)}

M. Kronberger,^{1,b)} D. Faircloth,² J. Lettry,¹ M. Paoluzzi,¹ H. Pereira,¹ J. Sanchez Arias,¹ C. Schmitzer,¹ and R. Scrivens¹

¹European Organisation for Nuclear Research, CERN, 1211 Geneva 23, Switzerland

²STFC, Rutherford Appleton Laboratory, Chilton, Oxon OX11 0QX, United Kingdom

(Presented 12 September 2011; received 10 September 2011; accepted 4 October 2011; published online 7 February 2012)

In the framework of the superconducting proton linac (SPL) study at CERN, a new non-cesiated H^- plasma generator driven by an external 2 MHz RF antenna has been developed and successfully operated at repetition rates of 50 Hz, pulse lengths of up to 3 ms, and average RF powers of up to 3 kW. The coupling efficiency of RF power into the plasma was determined by the cooling water temperatures and the analysis of the RF forward and reflected power and the antenna current and amounts to 50%–60%. The plasma resistance increases between 10 kW and 40 kW RF power from about 0.45 Ω to 0.65 Ω . Measurements of RF power dissipated in the ferrites and the magnets on a test bench show a 5-fold decrease of the power losses for the magnets when they are contained in a Cu box, thus validating the strategy of shielding the magnets with a high electrical conductivity material. An air cooling system was installed in the SPL plasma generator to control the temperatures of the ferrites despite hysteresis losses of several Watts. © 2012 American Institute of Physics. [doi:10.1063/1.3662478]

I. INTRODUCTION

In recent years, a possible expansion of the CERN accelerator complex by facilities producing intense neutrino and/or radioactive ion beams has been discussed. The multi-MW proton beam intensities required for operating such facilities could be delivered by the superconducting proton linac (SPL), a linear accelerator currently studied at CERN.¹ Using the currently constructed Linac4 (Refs. 2 and 3) as its front end, the SPL would accelerate H^- ions to energies of up to 5 GeV at 50 Hz repetition rate and pulse lengths of 0.4 to 0.8 ms.⁴

As part of the SPL study, a new H^- plasma generator⁵ has been developed from the RF powered, uncesiated DESY-Linac4 H^- source.⁶ In order to provide the nominal H^- current of 80 mA within a normalized rms beam emittance of 0.25 mm mrad foreseen for SPL, the plasma will be heated with up to 100 kW of 2 MHz forward RF power (P_{fwd}). Allowing for suppression of typically 100 μs beam head and tail instabilities, this gives a time average forward RF power $\langle P_{\text{fwd}} \rangle$ of up to 5 kW the plasma generator has to withstand during SPL operation.

II. SPL PLASMA GENERATOR AND TEST STAND

Figure 1 shows a cross section of the SPL plasma generator. H_2 gas is injected through a temperature stabilized piezo valve in the gas supply line. The gas pipe opens into a small, water-cooled ignition volume where the plasma is pre-ignited at the start of the RF pulse by an electric spark (900 V, 10 A, 50 μs). The 2 MHz RF pulse heating the plasma is produced by a water-cooled, epoxy insulated RF antenna coil

with $5\frac{1}{2}$ windings made of hollow-tube Cu and backed by ferrites. In order to match the 50 Ω impedance of the RF generator output, the antenna is connected to a high-Q resonant network containing a parallel and a series capacitor. An additional lumped coil in series with the antenna allows tuning the resonant circuit to 2 MHz.⁷ The matching network and the RF antenna share one cooling circuit to reduce the drift of the resonant frequency during high power runs. The AlN plasma chamber has a cooling circuit machined into the outer surface that is confined by a PEEK sleeve, assuring sufficient cooling for $\langle P_{\text{fwd}} \rangle$ of several kW. A multicusp arrangement of offset Halbach elements, each one made of three NdFeB magnets (type Vacodym 633HR, remanence $B_r = 1.33$ T) with different magnetization direction, confines the plasma. The cusp magnets are installed in a Cu magnet cage that shields them from RF-induced ohmic heating. Two magnet cages employing different multicusp configurations (octopole and dodecapole) are being tested. The extraction region contains two electrodes brazed together with AlN insulators for optimized heat transfer. A cooling circuit removes heat induced by the plasma. A dipole magnetic field created by two NdFeB magnets lowers the average electron energy in the collar region to improve H^- production and lower the electron current. The filter magnets are contained in Cu boxes to reduce ohmic heating induced by the 2 MHz RF.

The SPL plasma generator is mounted on a vacuum cross comprising six DN-160 flanges. Two of the flanges are connected to 500 l/s turbo molecular pumps in series with mechanical roughing pumps, while the remaining three flanges are used for monitoring of the vacuum pressure and for other diagnostics. The vacuum chamber, piezo valve, and cooling circuit temperatures are monitored by Pt-100 resistance thermometers. A LabView control and monitoring system constantly records all parameters with a slow time response, such as the vacuum and gas backing pressures and the

^{a)}Contributed paper, published as part of the Proceedings of the 14th International Conference on Ion Sources, Giardini Naxos, Italy, September 2011.

^{b)}Author to whom correspondence should be addressed. Electronic mail: matthias.kronberger@cern.ch.

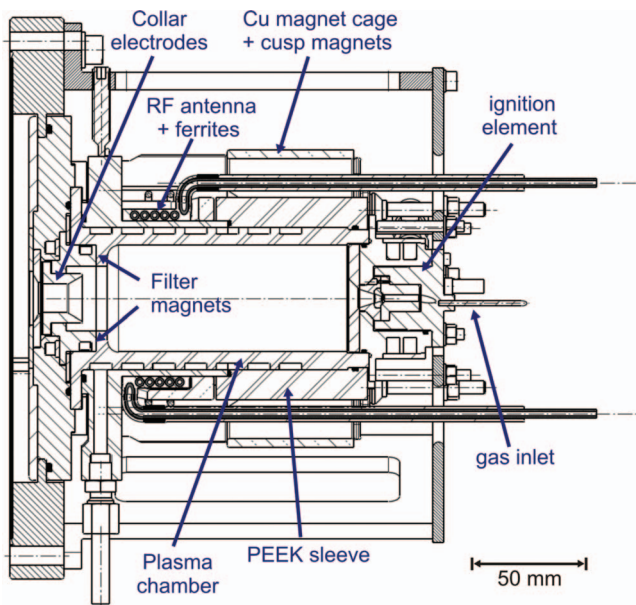


FIG. 1. (Color online) View of the SPL plasma generator (version 09/2011).

Pt-100 temperatures. An infrared camera (Fluke Ti-32) is used to map the temperatures of external surfaces and, through a Germanium window, the extraction region. A residual gas analyzer and a Langmuir probe system⁸ allow for gas and plasma diagnostics. An optical measurement system for plasma spectrometry at visual wavelengths and Balmer line photometry is described in Ref. 9. An extraction system comprising a puller electrode and two Faraday cups will be dedicated to electron and H^- current measurements.

III. PLASMA GENERATOR OPERATION AND THERMAL EQUILIBRIUM

The SPL plasma generator has been operated successfully at repetition rates of 50 Hz and pulse lengths of up to 3 ms. $\langle P_{fwd} \rangle = 3$ kW was reached on several occasions. In early tests, coronal discharges between the shrink tubes insulating the antenna tips, and sparking between the antenna windings were observed that at one occasion lead to antenna failure. These problems could be partly overcome by reinforcing the insulation of the antenna and increasing the distance to metallic components, however, operation is still limited to $P_{fwd} \leq 60$ kW. Moreover, alternative solutions for plasma ignition, such as the injection of microwaves or gas ionization by a radioactive source, are currently being investigated due to the high power demand on the electric spark gap that may lead to erosion of the electrodes.

All materials were found to operate well below their maximum operating temperatures, except for the collar electrode assembly where temperatures increased by >200 K at $\langle P_{fwd} \rangle = 3$ kW. A comparison with an ANSYS finite element (FE) thermal model showed that this could only be explained by assuming a very low thermal contact conductance between the electrode assembly and the adjacent components due to excessive tolerances. In order to improve the thermal contact in this region, three 0.1 mm thick Cu shims were installed. The

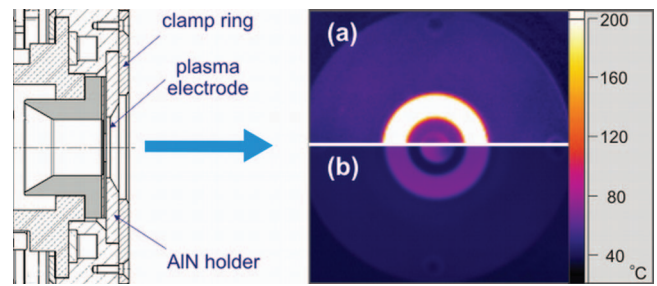


FIG. 2. (Color online) Temperature of the collar (a) before and (b) after insertion of three 0.1 mm thick Cu shims. Both images were corrected for the transmission t of the Germanium window ($t = 0.87$) and scaled on the emissivity ϵ of the AlN holder ($\epsilon = 0.9$). Note that plasma electrode and clamp ring have a considerably lower ϵ and thus, have their temperatures underestimated in the images. The left image shows a side view of the collar.

intervention reduced the temperature increase by 70%, in-line with the predictions from the thermal model (Fig. 2).

RF forward, reflected voltages, and antenna current I_{ant} were analyzed during the tests with a MATLAB script⁷ to determine P_{fwd} and the reflected RF power P_{ref} , the contribution of the plasma to the circuit inductance (L_{pl}) and resistance (R_{pl}), and the power deposited in the plasma and the matching circuit. The data show that R_{pl} increases from about 0.45 to 0.65 Ω for P_{fwd} between 10 and 40 kW when the system is optimally matched (Fig. 3(a)). For P_{ref} , values of typically 0.1 P_{fwd} are observed. The RF data suggest a coupling efficiency of RF power into the plasma of 50%–60% which is in excellent agreement with an independent estimate from the temperature increase observed in the cooling circuits (Fig. 3(b)). The analysis of the cooling water temperatures also shows that more than 80% of the power coupled into the plasma is dissipated into the AlN plasma chamber cooling circuit, which is in good agreement with the value derived from a simple plasma heating model used to model the thermal flow in the Linac4 and SPL plasma generators.¹⁰

IV. RF HEATING OF MAGNETIC COMPONENTS

A potential problem for high power operation is the overheating of the cusp and filter magnets due to RF-induced ohmic losses. Further investigation showed that the problem

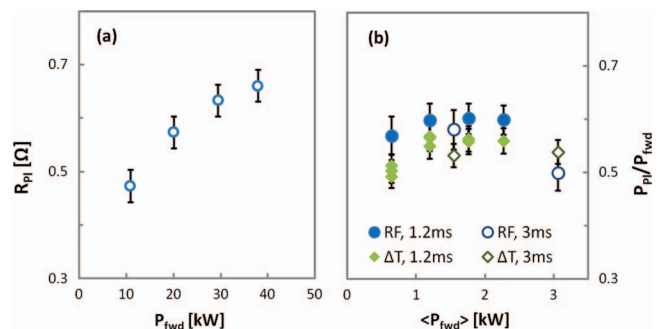


FIG. 3. (Color online) (a) Development of plasma resistance R_{pl} with P_{fwd} . (b) Fraction of RF power deposited in the plasma as a function of $\langle P_{fwd} \rangle$ derived from RF data (blue circles) and from the increase of the cooling water temperature ΔT (green stars). Filled symbols correspond to measurements at 1.2 ms pulse length, open symbols to 3 ms pulse length.

may be mitigated by shielding the magnets with a low resistivity material, such as copper.¹¹ Similar conclusions were found for the ferrites, which are expected to heat up considerably due to hysteresis losses.

The power P_{diss} dissipated in the cusp magnets and the ferrites during SPL operation was assessed by test bench¹¹ measurements employing the same RF system and antenna geometry as the SPL plasma generator. The tests were conducted with two different types of ferrites (4L, 8C11) and two Ni-coated, N-S magnetized NdFeB magnets of the same dimensions as the cusp Halbach elements used in the SPL plasma generator. In order to assess the shielding effect of Cu against RF-induced ohmic losses, one of the magnets was placed inside a Cu box. Distances and positions of magnets and ferrites were identical to the SPL plasma generator. Black paint was used to uniformize the emissivities of the IR-monitored surfaces. The observed temperature distributions were used to benchmark a FE thermal model of the test bench which yielded P_{diss} . An additional electromagnetic FE model of the test bench simulated with Vector Fields Opera provided an independent estimate of the ohmic losses in the magnets.

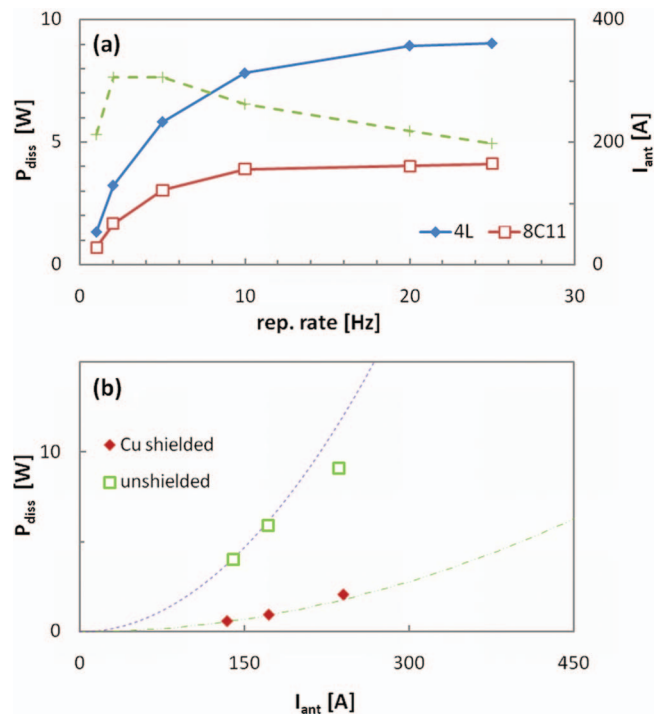


FIG. 4. (Color online) (a) Power P_{diss} dissipated in the 4L and 8C11 ferrites due to hysteresis losses. The dashed curve gives the value of I_{ant} measured during each measurement. (b) Power P_{diss} dissipated in the unshielded and shielded magnets vs. I_{ant} . The dashed curves show P_{diss} vs. I_{ant} calculated from an electromagnetic FE model.

The results show that both types of ferrites reach their Curie temperatures T_C of, respectively, 240 °C (4L) and 120 °C (8C11) already at 1 ms pulse length and 25 Hz repetition rates for $I_{\text{ant}} = 200$ A, which is typically the value for $P_{\text{fwd}} = 20$ kW in the SPL plasma generator. The power losses per ferrite obtained by the thermal model are significant and reach several Watts (Fig. 4). The temperature increase observed in the Cu-protected magnets is considerably lower than in the unprotected magnets. The thermal and the electromagnetic models are in good to excellent agreement with each other. According to both models, P_{diss} is 5 to 6 times lower for the Cu-shielded magnet than for the unshielded magnet (Fig. 4), thus validating our approach of shielding the magnets from RF-induced ohmic losses. The necessity of shielding the magnets from the RF is also illustrated by precision measurements of the magnetic field strength B before and after the experiments that revealed a decrease of B of the order of 50% for the unshielded magnet.

The problem of ferrite heating was successfully addressed by installing a compressed air cooling system in the SPL plasma generator that keeps their temperatures at a reasonable level during operation. In future experiments, the problem of overheating may be mitigated by using soft magnetic compounds with lower hysteresis losses.

ACKNOWLEDGMENTS

This project has received funding from the European Community's Seventh Framework Programme (FP7/2007-2013) (Grant Agreement No. 212114).

- ¹M. Baylac, F. Gerigk, E. Benedico-Mora, F. Caspers, S. Chel, J. M. Deconto, R. Duperrier *et al.*, CERN Report No. 2006-006, 2006.
- ²M. Vretenar, in *Proceedings of Linear Accelerator Conference LINAC2010*, Tsukuba, Japan, 12–17 September 2010, p. WE 103–107.
- ³L. Arnaudon, P. Baudrengnien, M. Baylac, G. Bellodi, Y. Body, J. Borburgh, P. Bourquin, *et al.*, CERN-AB Report No. 2006-084, 2006.
- ⁴F. Gerigk, G. Arnau, S. Atieh, S. Calatroni, R. Calaga, O. Capatina, E. Ciapala, *et al.*, in *Proceedings of Linear Accelerator Conference LINAC2010*, Tsukuba, Japan, 12–17 September 2010, pp. THP004.
- ⁵J. Lettry, M. Kronberger, R. Scrivens, E. Chaudet, D. Faircloth, G. Favre, J.-M. Geisser, *et al.*, *Rev. Sci. Instrum.* **81**, 02A723 (2010).
- ⁶D. Küchler, T. Meinschad, J. Peters, and R. Scrivens, *Rev. Sci. Instrum.* **79**, 02A504 (2008).
- ⁷M. Paoluzzi, M. Haase, J. M. Balula, and D. Nisbet, *AIP Conf. Proc.* **1390**, 265 (2011).
- ⁸C. Schmitzer, M. Kronberger, J. Lettry, J. Sanchez Arias, and H. Störi, “Plasma characterisation of the SPL plasma generator using a 2 MHz compensated Langmuir probe,” *Rev. Sci. Instrum.* (these proceedings).
- ⁹J. Lettry, U. Fantz, M. Kronberger, T. Kalvas, H. Koivisto, J. Kompulla, E. Mahner, *et al.*, “Optical emission spectroscopy of the Linac4 and SPL plasma generators,” *Rev. Sci. Instrum.* (these proceedings).
- ¹⁰D. Faircloth, M. Kronberger, D. Küchler, J. Lettry, and R. Scrivens, *Rev. Sci. Instrum.* **81**, 02A722 (2010).
- ¹¹M. Kronberger, E. Chaudet, G. Favre, J. Lettry, D. Küchler, P. Moyret, M. Paoluzzi, *et al.*, *AIP Conf. Proc.* **1390**, 255 (2011).